Talanta 79 (2009) 780–786

Contents lists available at ScienceDirect

Talanta

journal homepage: www.elsevier.com/locate/talanta

Direct electrochemistry and electrocatalysis of hemoglobin immobilized in a magnetic nanoparticles-chitosan film

Na Zheng, Xia Zhou, Weiying Yang, Xiangjun Li*, Zhuobin Yuan

College of Chemistry and Chemical Engineering, Graduate University of Chinese Academy of Sciences, Beijing 100049, China

ARTICLE INFO

Article history:
Received 4 March 2009
Received in revised form 27 April 2009
Accepted 4 May 2009
Available online 12 May 2009

Keywords:
Fe_3O_4 nanoparticles
Direct electrochemistry
Electrocatalysis
Hemoglobin
Hydrogen peroxide

ABSTRACT

Magnetic nanoparticles (Fe_3O_4) were synthesized by a chemical coprecipitation method. X-ray diffraction (XRD) and transmission electron microscope (TEM) were used to confirm the crystallite structure and the particle's radius. The Fe_3O_4 nanoparticles and chitosan (CS) were mixed to form a matrix in which haemoglobin (Hb) can be immobilized for the fabrication of H_2O_2 biosensor. The Fe_3O_4–CS–Hb film exhibited a pair of well-defined and quasi-reversible cyclic voltammetric peaks due to the redox of Hb–heme Fe (III)/Fe (II) in a pH 7.0 phosphate buffer. The formal potential of Hb–heme Fe(III)/Fe(II) couple varied linearly with the increase of pH in the range of 4.0–10.0 with a slope of 46.5 mV pH^{-1}, indicating that electron transfer was accompanied with single proton transportation in the electrochemical reaction. The surface coverage of Hb immobilized on Fe_3O_4–CS film glassy carbon electrode was about 1.13×10^{-10} mol cm^{-2}. The heterogeneous electron transfer rate constant (k_s) was 1.04 s^{-1}, indicating great facilitation of the electron transfer between Hb and magnetic nanoparticles-chitosan modified electrode. The modified electrode showed excellent electrocatalytic activity toward oxygen and hydrogen peroxide reduction. The apparent Michaelis–Menten constant K_M^{app} for H_2O_2 was estimated to be 38.1 μmol L^{-1}.

1. Introduction

Direct electrochemistry of redox proteins or enzymes has been the research focus for many years in views of the good model for mechanistic studies of their electron transfer activity in biological systems and serves as a foundation for fabricating electrochemical biosensors and bioreactors without using chemical mediators [1,2]. Unfortunately, because of the deep bury of the electroactive prosthetic groups, the adsorptive denaturation of proteins onto electrodes and the unfavorable orientations at electrodes, the proteins or enzymes exhibit a rather slow rate of heterogeneous electron transfer at conventional electrodes, although their electron transfer is quite fast in biological systems [3]. Generally, modification of the electrodes' surfaces by deposition of various films, including self-assembled monolayers (SAMs) [4], electropolymerization [5], layer by layer assembly [6], covalent-bonded immobilization [7] is an effective way to enhance the rate of electron transfer and obtain direct electrochemistry of redox enzymes or proteins. Successful examples have included cast films of proteins with insoluble surfactants [8], hydrogel polymers [9], biopolymers [10], clay [11], etc.

Recently, nanoparticles have attracted increasing attention because the nanoparticles could adsorb redox enzymes and proteins without loss of their biological activity. In addition, the electron transfer activity and biocatalytic activity of enzymes increased when they were adsorbed on nanomaterials [12]. Many metal oxide nanoparticles such as copper oxide [13], zinc oxide [14], titanium oxide [15], zirconium oxide [16] are used successfully for immobilization and direct electrochemistry of enzymes and proteins. Fe_3O_4 nanoparticles have been used to immobilize enzymes [17,18], because of their good biocompatibility, strong superparamagnetic property, low toxicity and easy preparation [19–21], especially, magnetite is found to exist in the human brain, the particles of this materials are generally smaller than 200 nm, and, in most cases, are on the order of a few tens of nanometers [22,23]. So, it is meaningful to study the bioactivity and biocatalysis of enzymes and proteins when they are entrapped in the Fe_3O_4 nanoparticles.

Hemoglobin (Hb), an important redox respiratory protein in red cells, has a molecular weight of approximately 64,500. It contains the porphyrin complex of iron (II) or hemin (III) as a prosthetic group and has four electroactive heme redox centers in its respective four polypeptide chains. It is reported that hemoglobin can be used as a substitute of horseradish peroxidase (HRP) to catalyze the reduction of peroxide hydrogen [24], and it is also an ideal model protein for studying the electron transfer of heme molecules.

However, when nanoparticles such as Fe_3O_4 are used to immobilized proteins and enzymes, the tendency to aggregation of nanoparticles limits their further applications, so it is necessary to disperse Fe_3O_4 in a suitable matrix to prevent aggregation. Chitosan

* Corresponding author. Tel.: +86 010 88256336; fax: +86 010 88256336.
E-mail address: lixiangj@gucas.ac.cn (X. Li).

0039-9140/$ – see front matter © 2009 Elsevier B.V. All rights reserved.
doi:10.1016/j.talanta.2009.05.002

(CS) is a kind of natural polysaccharide, which is derived from chitin, has good biocompatibility, biodegradability, low toxicity, haemostatic potential, good film forming character and anti-infectional activity [25]. Due to its desirable properties, chitosan has been widely used for electrochemical biosensing platforms combined with metal nanoparticles [26], carbon nanotubes [27] and ionic liquids [28]. Moreover, the CS can facilitate the immobilization of enzymes like Hb because it contains primary amino groups which provide a hydrophilic environment compatible with the biomolecules [29]. The isoelectric point of CS is around pH 8.5 [30]. So CS has positive charges in solutions [31]. With the isoelectric point at 5.9 [32], Fe_3O_4 nanoparticles have negative surface charges at pH 8.0. In this research, Fe_3O_4–CS composites were constructed by electrostatic interactions between positively charged CS particles and negatively charged Fe_3O_4.

In this paper, we studied the direct electron transfer and electrocatalysis of Hb in the Fe_3O_4–CS interfaces. The Hb embedded in the Fe_3O_4–CS was characterized by the UV–vis and FTIR spectroscopy to indicate that the secondary structure of Hb was not destroyed and retained its biological activity. The electrode modified with Fe_3O_4–CS–Hb film had high stability and displayed significant biological activities. The electrocatalytic reduction of oxygen and hydrogen peroxide in this electrode has been observed, showing the possible potential application of the film as the third generation biosensor of hydrogen peroxide.

2. Experimental

2.1. Chemicals and materials

Bovine hemoglobin (Hb, MW 64,500) purchased from Sigma Chemical Co. was used without further purification. Hydrogen peroxide (H_2O_2, 30%) was obtained from Beijing Chemical Works (Beijing, China). Chitosan (molar weight $\sim 1 \times 10^6$, 75–85% deacetylation) was supplied by Sigma (St. Louis, MO, USA). Other chemicals were of analytical reagent grade. Phosphate buffer solutions (PBS) were prepared by 0.1 M KH_2PO_4 and 0.1 M K_2HPO_4, and the pH was adjusted with 0.1 M H_3PO_4 or 0.1 M NaOH. All aqueous solutions were prepared in doubly distilled water.

2.2. Synthesis of Fe_3O_4 nanoparticles

Fe_3O_4 nanoparticles were self-synthesized according to the literature [33]. In a typical process, deionizated water was placed in a 3-neck round-bottom flask and deoxygenated by bubbling N_2 for 30 min. Then certain concentrated ferrous chloride hexa-hydrate ($FeCl_3 \cdot 6H_2O$) and ferric chloride tetra-hydrate ($FeCl_2 \cdot 4H_2O$) aqueous solutions were added. Later certain concentrated ammonium hydroxide (NH_4OH) in the long-stem funnel was added with vigorous stirring until the pH of the mixture reached above 10 and the reaction continued for 30 min in a constant temperature water bath. The product was washed several times with deionizated and deoxygenated water, then dried in vacuum at 60 °C for 12 h. Finally Fe_3O_4 nanoparticles were obtained.

2.3. Apparatus and electrochemical measurements

The structure and morphology of Fe_3O_4 nanoparticles were characterized by a X-ray diffractometer (XRD, MSAL XD-2 powder X-ray diffractometer using Cu Kα radiation of wavelength 1.5406 Å at 30 kV and 30 mA) and transmission electron microscopy (TEM, H800, Hitachi Instrument Co., Japan). The image of the modified electrode was characterized by scanning electron microscopy (SEM, KYKY-2800 microscope, KYKY Technology Development Ltd., China) at an accelerating voltage of 20 keV. X-ray photoelectron spectroscopy data were obtained with an ESCALab220i-XL electron spectrometer from VG Scientific using 300W Al Kα radiation. The UV–vis absorption spectroscopy study was carried out using a UV–vis 2550 Spectrophotometer (Shimadzu, Kyoto, Japan). FTIR spectra were recorded with Nicolet 360v FTIR spectrophotometer (Nicolet Instrumental, USA).

The electrochemical measurements were carried out using a computer-controlled electrochemical analyzer (CHI 660A, CH Instruments, Austin, TX, USA) with a three-electrode cell. The Fe_3O_4–CS–Hb/GCE was used as the working electrode, a platinum wire as the counter electrode, and a saturated calomel electrode (SCE) as the reference electrode. All potentials were quoted with respect to SCE. Phosphate buffer (0.1 M pH 7.0) was used as the supporting electrolyte. All experimental solutions were thoroughly deoxygenated by bubbling high-purity nitrogen and maintained under nitrogen atmosphere during measurements. All electrochemical measurements were performed at ambient temperature 18 ± 2 °C.

2.4. Preparation of the Fe_3O_4–CS–Hb/GCE

Prior to coating, glassy carbon electrode (GCE, diameter 3.0 mm) was polished before each experiment with 1.0, 0.30 and 0.05 μm α-alumina powder and sonicated in 1:1 nitric acid, ethanol, doubly distilled water in turn, and then dried at room temperature. The Fe_3O_4–CS–Hb/GCE was prepared as follows. The aqueous dispersion of Fe_3O_4 nanoparticles was prepared by vigorous stirring for about 8 h in pH 8.0 buffer. The suspension was stirred for 30 min just before preparing the films. Then CS (dissolved in acetic acid solution), which is served as a dispersant to prevent Fe_3O_4 nanoparticles aggregation, was added into aqueous. Later Hb solution was added to the suspension and stirred for 30 min. The Hb molecules were absorbed on the surface of CS during mixing. Then, 3 μL of the resulting mixture was pipetted onto the surface of GCE. A small plastic bottle was fitted tightly above the electrode surface to serve as a closed evaporation chamber, to make sure the solvent evaporated slowly and more uniform film formed. The film was dried at 4 °C overnight in air and the Fe_3O_4–CS–Hb/GCE was obtained. If it was not used immediately, the electrode was stored at 4 °C in a refrigerator. In the above procedure, if Fe_3O_4 nanoparticles were absent, the electrode obtained was the Hb–CS/GCE.

3. Results and discussion

3.1. Structural and morphology characterization of Fe_3O_4 nanoparticles

The structure of the as-obtained product was firstly characterized by X-ray diffraction (XRD) (Fig. 1). The strong diffraction peaks at 2θ angles of 30°, 35°, 42° and 62.5° may correspond to the crystal plane of (2 2 0), (3 1 1), (4 0 0) and (4 4 0) of the cubic phase. All peaks were consistent with that reported previously [33]. According to Scherrer formula, the average diameter of prepared Fe_3O_4 is about 8.8 nm.

TEM was used to view the size of Fe_3O_4 particles in aqueous dispersions (Fig. 2A), showing that the average particle size of Fe_3O_4 was 40 nm. This size was larger than the size of 8.8 nm obtained by XRD, indicating some extent of aggregation of the particles.

3.2. Characterization of modified film by SEM

In order to investigate the formation of the modified film, SEM image of Fe_3O_4–CS film on ITO glass was given in Fig. 2B. It shows that Fe_3O_4 nanoparticles are well dispersed, which could confirm

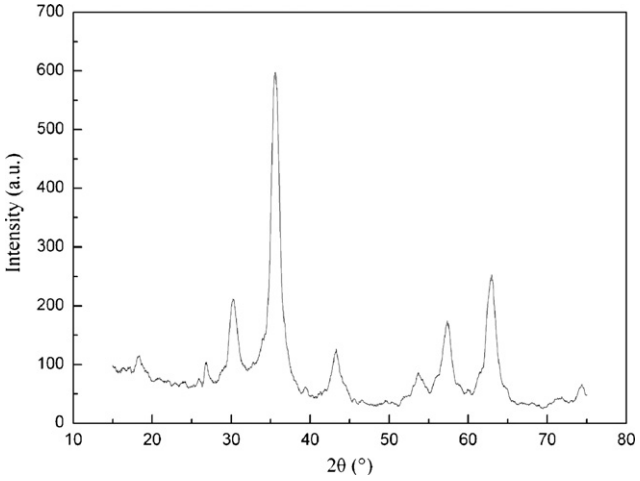

Fig. 1. XRD patterns taken from the Fe_3O_4 samples prepared.

that Fe_3O_4 nanoparticles have been successfully entrapped in the chitosan film.

3.3. Conformational studies of Hb

In order to confirm the existence of Hb on the surface of Fe_3O_4–CS composite, XPS experiment was carried out. Fig. 3A shows the XPS spectrum of Hb immobilized on the surface of Fe_3O_4–CS composite in the N1s regions. It can be observed that the characteristic peak of N1s of N was at 399.9 eV (Fig. 3A). Since N is from Hb, the result indicated the existence of Hb on the surface of Fe_3O_4–CS composite.

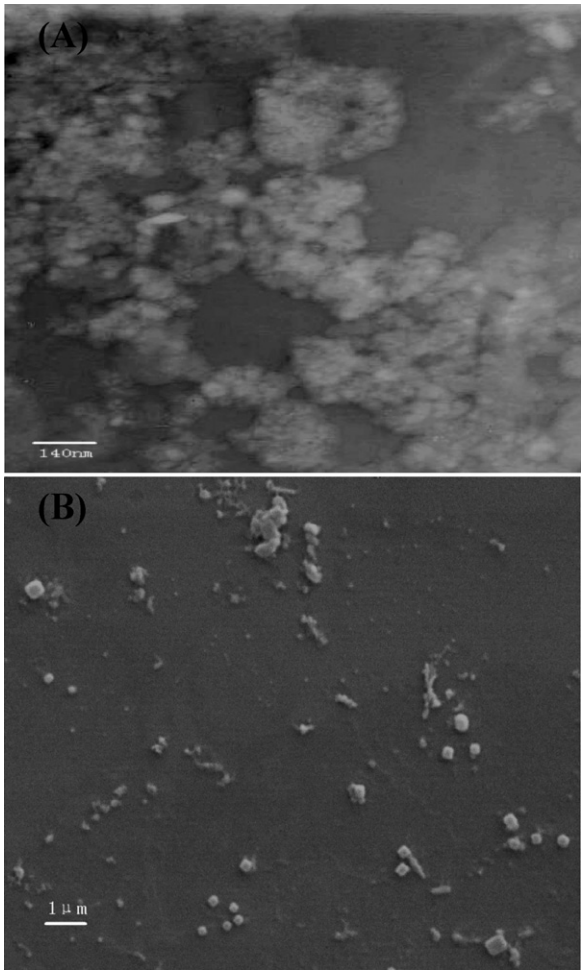

Fig. 2. (A) TEM image of Fe_3O_4 nanoparticles in aqueous dispersions. Scale bar: 140 nm. (B) SEM image of Fe_3O_4–CS film.

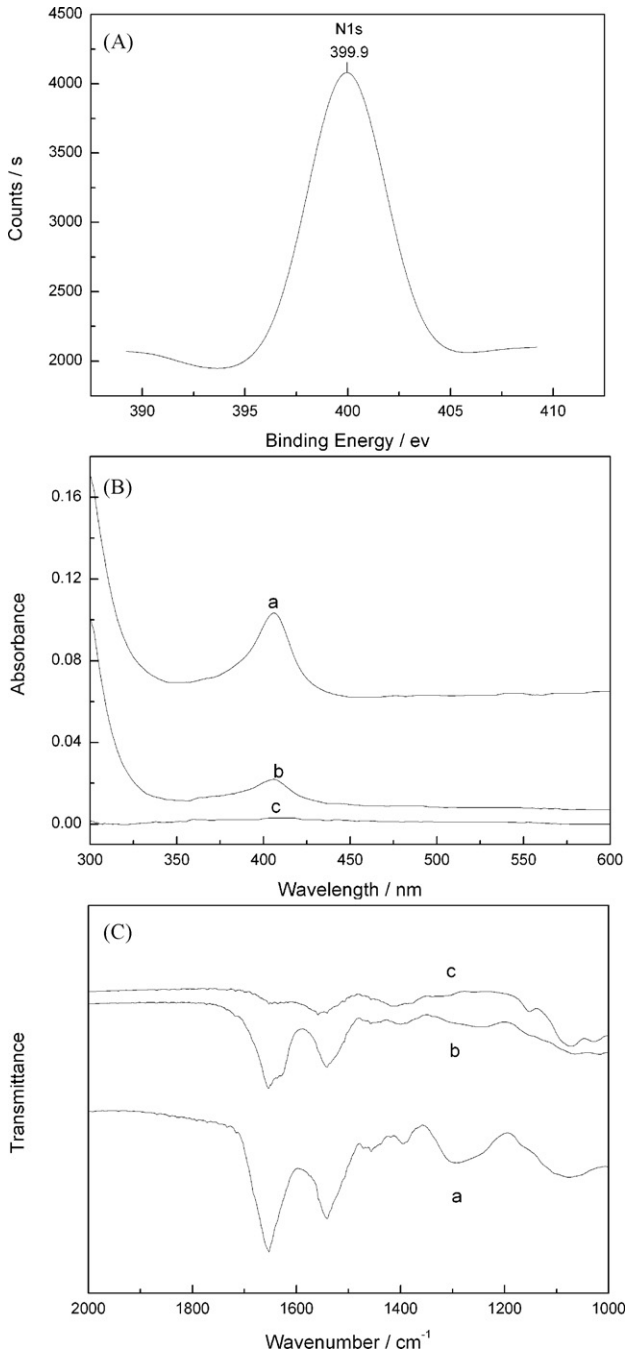

Fig. 3. (A) The XPS spectrum of Hb immobilized on the surface of Fe_3O_4–CS composite in N1s region. (B) UV–vis spectra of Hb (a), Fe_3O_4–CS–Hb (b) and Fe_3O_4–CS composite (c). (C) FTIR spectra of Hb (a), Fe_3O_4–CS–Hb (b) and Fe_3O_4–CS composite (c).

UV–vis spectroscopy is a conventional tool for monitoring the possible change of the Soret absorption band in the heme group region. The band shift may provide the information of possible denaturation of heme protein, particularly conformational change [34]. Fig. 3B shows the UV–vis spectra of Hb (Fig. 3B(a)), Fe_3O_4–CS–Hb (Fig. 3B(b)) and Fe_3O_4–CS composite (Fig. 3B(c)) in pH 7.0 PBS, respectively. The Soret band of Fe_3O_4–CS–Hb appeared

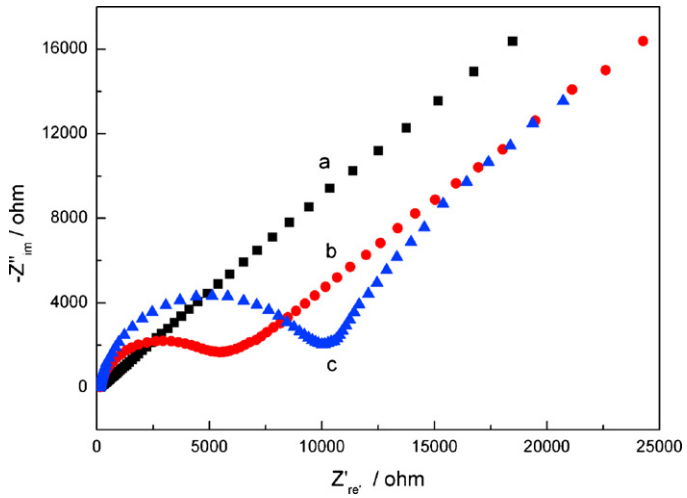

Fig. 4. EIS of: bare GCE (a); Fe_3O_4/GCE (b) and Fe_3O_4–CS–Hb/GCE (c) in 0.1 mol L^{-1} KCl containing 1 mmol L^{-1} $K_3[Fe(CN)_6]$.

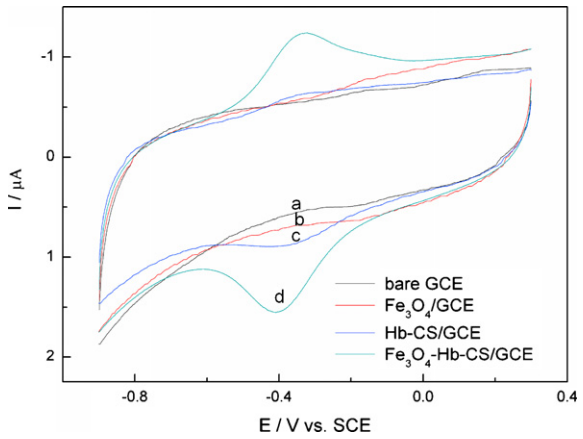

Fig. 5. Cyclic voltammograms of bare GCE (a), Fe_3O_4/GCE (b), Hb–CS/GCE (c), Fe_3O_4–CS–Hb/GCE (d) in 0.1 M pH 7.0 PBS. Scan rate: 200 mV s^{-1}.

at 405 nm (Fig. 3B(b)), the same as that of native Hb in phosphate buffer (Fig. 3B(a)), indicating that the secondary structure of Hb immobilized on the surface of Fe_3O_4–CS was not destroyed and Hb retained its biological activity.

The immobilization of Hb on the surface of Fe_3O_4–CS did not alter the structure of Hb. This conclusion can also be verified by the FTIR spectra. Fig. 3C(a) is the FTIR spectrum of Hb. The amide I band of Hb, which was caused by C=O stretcthing vibrations of peptide linkages, appeared at 1653 cm^{-1}. The signal at 1541 cm^{-1} indicated the characteristic of amide II, which resulted from a combination of N–H in plane bending and C–N stretching vibrations of the peptide groups. The characteristic amide I and II bands of proteins provide detailed information on the secondary structure of polypeptide chain [35]. Fig. 3C(b) is the FTIR spectrum of Fe_3O_4–CS–Hb. The amide I (1654 cm^{-1}) and II (1541 cm^{-1}) bands appeared essentially the same positions as those of free Hb, suggesting an unchanged secondary structure for the intercalated Hb.

In electrochemical impedance spectroscopy (EIS), the impedance change of the electrode surface can characterize the stepwise-assemble process of the surface-modified electrode. In EIS, the semicircle part at higher frequencies corresponds to the electron-transfer limited process; its diameter is equal to the electron transfer resistance, R_{et}, which controls the electron transfer kinetics of the redox probe at the electrode interface. At bare GCE, an almost straight line could be observed (Fig. 4a), showing a diffuse limiting step of the electrochemical processes. After dripping Fe_3O_4 nanoparticles on the surface of the electrode, an obvious interfacial R_{et} was observed (Fig. 4b). This may be ascribed to the film's weak conductivity. When Hb–CS was assembled onto the Fe_3O_4 membrane, the R_{et} increased obviously (Fig. 4c), which proved the successful assemble of Hb–CS.

3.4. Direct electrochemistry of Fe_3O_4–CS–Hb/GCE

Fig. 5 shows the cyclic voltammograms of bare GCE (a), Fe_3O_4/GCE (b), Hb–CS/GCE (c) and Fe_3O_4–CS–Hb/GCE (d) in deaerated 0.1 M pH 7.0 PBS at a scan rate of 200 mV s^{-1}. No redox peaks were observed in the cyclic voltammogram of the bare GCE and Fe_3O_4/GC electrode (Fig. 5a and b), indicating that Fe_3O_4 was non-electroactive. When the electrode was modified with Hb–CS, the redox peaks of Hb could be observed (Fig. 5c), but the current was much less than Fe_3O_4–CS–Hb/GCE, suggesting that the direct electron thansfer was difficult between Hb and the electrode. A pair of well-defined and nearly symmetrical redox peaks was observed at the Fe_3O_4–CS–Hb/GCE (Fig. 5d), indicating that Fe_3O_4 nanoparticles in the film could increase the adsorption ability for Hb and favor the orientation of Hb. It was no doubt that the pair peaks arose from Hb entrapped in the composite film. The anodic peak potential (E_{pa}) and cathodic peak potential (E_{pc}) were located at −0.324 and −0.412 V, respectively. Its formal potential (defined as the average of E_{pa} and E_{pc}), $E^{0\prime}$ was −0.368 V vs. SCE, a characteristic of the Hb–heme Fe(III)/Fe(II) redox couple. Thus, this also suggested that Hb immobilized on Fe_3O_4–CS did not denature. The separation of peak potentials ($\Delta E_p = E_{pa} - E_{pc}$) was 88 mV at a scan rate of 200 mV s^{-1}, and almost unchanged with the increase of v. So Fe_3O_4–CS film provided a better microenvironment for Hb to undergo a facile electron transfer reaction. The results implied that the electron transfer rate between Hb and GCE was relative fast. Moreover, the ratio of the cathodic current to the anodic current was close to one. These electrochemical parameters suggested that Hb underwent a quasi-reversible redox process at Fe_3O_4–CS–Hb/GCE, which can also attributed to the synergistic promotion action of Fe_3O_4 and CS.

According to Faraday laws, $\Gamma^* = Q/nFA$, where Q is the charge involved in the reaction, n is the number of electron transferred, F is the Faraday constant and A is the effective area of the GCE, the surface concentration of electroactive Hb (Γ^*) was calculated to be 1.13×10^{-10} mol cm^{-2} for Fe_3O_4–CS–Hb/GCE. The value was larger than the theoretical monolayer coverage of Hb (1.89×10^{-11} mol cm^{-2}) [36] on the basis of the crystallographic dimensional structure of Hb and assuming that the biomolecule adopts an orientation with the long axis parallel to the electrode surface [37]. The bigger surface coverage can be ascribed to the expanded interspace to hold more Hb molecules, indicating that intercalated Hb in the composited film participated in the electron transfer process. Therefore, the present Fe_3O_4 nanoparticles is a promising material for increasing the functional density of Hb, allowing the electric communication with the underlying GCE. According to the Laviron equation [38],

$$I_p = \frac{n^2F^2Av\Gamma}{4RT} = \frac{nFQv}{4RT}$$

the number n of electrons involved in the direct electron transfer reaction of Hb was calculated to be $n = 0.90$, indicating that the redox reaction of the adsorbed Hb on the Fe_3O_4 modified electrode was a single electron transfer reaction.

The typical cyclic voltammograms of Fe_3O_4–CS–Hb/GCE in pH 7.0 PBS at different scan rates are shown in Fig. 6. The electrode modified with the Fe_3O_4–CS–Hb composite displayed well-defined peaks and showed almost equal height of reduction and oxidation peaks at the same scan rate. With the increase of the scan rate,

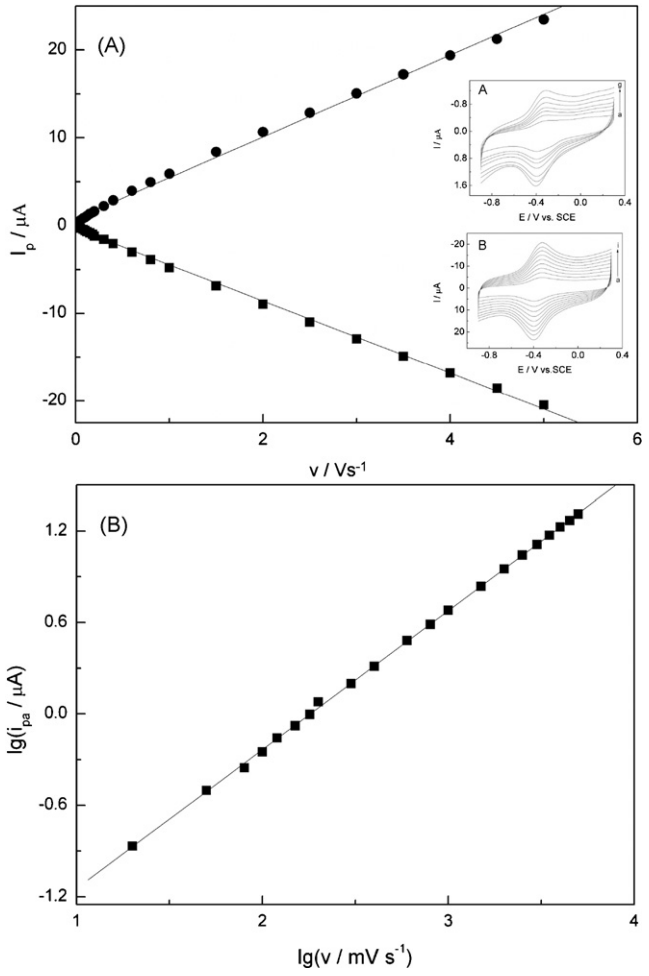

Fig. 6. (A) Plots of peak current vs. scan rate from Fig. 9 inset A, B. Inset A: Cyclic voltammograms of Fe_3O_4–CS–Hb/GCE in 0.1 M pH 7.0 PBS at the low scan rate of (a) 50, (b) 80, (c) 100, (d) 120, (e) 150, (f) 180, (g) 200 mV s^{-1}. Inset B: Cyclic voltammograms of Fe_3O_4–CS–Hb/GCE in 0.1 M pH 7.0 PBS at the high scan rate of (a) 1000, (b) 1500, (c) 2000, (d) 2500, (e) 3000, (f) 3500, (g) 4000, (h) 4500, (i) 5000 mV s^{-1}. (B) Plot of logarithm of I_{pa} vs. logarithm of v.

the cathodic and anodic peak currents increased simultaneously in Fig. 6(A). Furthermore, integration of reduction peaks at different scan rates gave nearly constant charge (Q) values which indicated a surface-controlled process, in which nearly all electroactive proteins in the films are reduced on the forward cathodic scan, with full conversion of the reduced proteins back to their oxidized forms on the reversed anodic scan. The slope obtained by linear regression of log I_{pa} vs. log v was 0.91 for Hb (Fig. 6(B)), which corresponded to the characteristic of a thin-layer electrochemical behavior. The potential separation between anodic and cathodic peaks (ΔE_p) was larger than the theoretical value of 0 mV for a surface process, which was probably attributed to the long distance between the heme of Hb and the electrode surface for the deep-buried electroactive centers in polypeptides.

The electron transfer rate constant k_s can be estimated with equation $k_s = mnFv/RT$ when the peak-to-peak separation is less than 200 mV [38], where m is a parameter related to the peak-to-peak separation. The k_s value was calculated to be 1.04 s^{-1} at the scan rate of 150 mV s^{-1}, which was larger than that of Hb immobilized on Au–colloid–cysteamine-modified gold electrode (0.49 s^{-1}) [39], Hb modified CNT powder microelectrodes electrodes (0.062 s^{-1}) [40]. Thus, Fe_3O_4 can provide a microenvironment for Hb to undergo a facile electron transfer reaction.

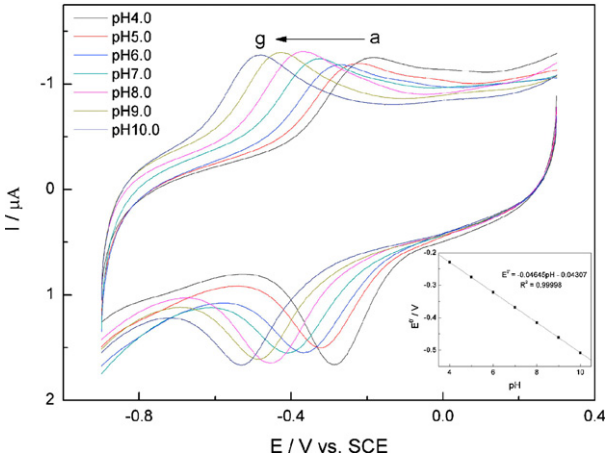

Fig. 7. Cyclic voltammograms of the Fe_3O_4–CS–Hb/GCE in 0.1 M pH7.0 PBS at pH: (a) 4.0, (b) 5.0, (c) 6.0, (d) 7.0, (e) 8.0, (f) 9.0 and (g) 10.0. Scan rate: 200 mV s^{-1}. Inset: the plot $E^{0\prime}$ of Hb vs. pH of the solution.

3.5. Effect of solution pH on peak potential of Hb at Fe_3O_4–CS–Hb/GCE

In most cases, the solution pH is essential to the electrochemical behaviors of proteins. Generally, the $E^{0\prime}$ of the redox couple depends on the solution pH which indicates the participation of proton in the redox process. The cyclic voltammograms of Fe_3O_4–CS–Hb/GCE at different pH solutions were measured at a scan rate of 200 mV s^{-1} (Fig. 7). A pair of stable and well-defined redox peaks were obtained. An increase of solution pH caused a negative shift in both cathodic and anodic peak potentials for Hb, indicating that proton was involved in the electrode reaction of Hb. $E^{0\prime}$ shifted linearly to the negative direction with a slope −46.5 mV pH^{-1} by increasing pH, which was a bit smaller than the theoretical value −57.6 mV pH^{-1} at 18 °C for a reversible one proton coupled single-electron transfer [41]. This may be owing to the effect of the protonation states of trans ligands to the heme iron and amino acids around the heme or to the protonation of water molecules coordinated to the center [42] that may exist in different states under different pH values. Thus, the electron-transfer between Hb and the electrode can be presented by

$$\text{HbhemeFe(III)} + \text{H}^+ + \text{e}^- \leftrightarrow \text{HbhemeFe(II)}$$

3.6. Electrocatalysis of Hb in Fe_3O_4–CS film

It is well known that proteins and enzymes containing the heme group, such as horseradish peroxidase, cytochrome c, hemoglobin and myoglobin, have the ability to reduce O_2 and H_2O_2 electrocatalytically. In order to estimate the electrochemical catalytic activity of Fe_3O_4–CS–Hb/GCE for the reduction of O_2 and H_2O_2, the cyclic voltammetry has been performed.

When the solution was deoxygenated thoroughly, a pair of well-defined redox peaks can be obtained with almost the equal height of the reduction and oxide peaks (Fig. 8A(b)). However, when Fe_3O_4–CS–Hb/GCE was dipped in a pH 7.0 PBS without deaerating O_2, only a significant reduction peak at about −0.32 V was observed while oxidation peak of Hb Fe(II) disappeared (Fig. 8A(d)), suggesting that Hb Fe (II) reacted with oxygen. For Fe_3O_4/GC, the reduction peak of oxygen was observed at about −0.81 V (Fig. 8A(c)), far more negative than the catalytic peak potential. Therefore, the over-potential required for reduction of O_2 was lowered by about 0.5 V by Fe_3O_4–CS–Hb film. Catalytic efficiency (defined as the ratio of reduction peak current in the presence (I_c) and absence (I_d) of oxygen, I_c/I_d) decreased with increasing the scan rate for

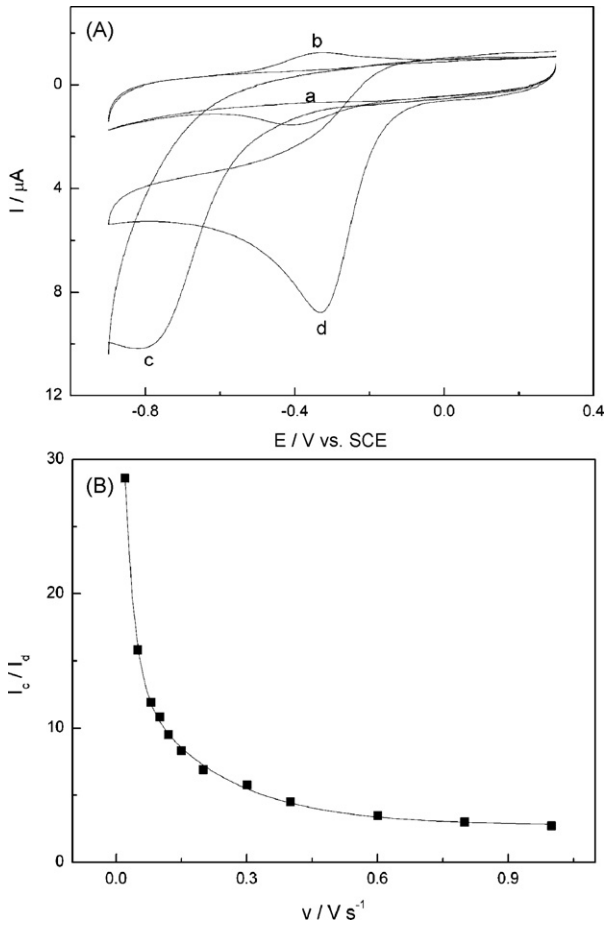

Fig. 8. (A) Cyclic voltammograms in 0.1 M pH 7.0 PBS at 200 mV s^{-1} for Fe_3O_4/GCE (a), Fe_3O_4–CS–Hb/GCE (b) without oxygen present, Fe_3O_4/GCE (c), Fe_3O_4–CS–Hb/GCE (d) with oxygen present. (B) Influence of scan rate on catalytic efficiency, I_c/I_d, for Fe_3O_4–CS–Hb film in pH 7.0 PBS buffer, where I_c is the CV reduction peak current in buffers with air and I_d is the CV reduction peak current in buffers without oxygen.

Fe_3O_4–CS–Hb/GC electrode (Fig. 8B), also a characteristic of electrochemical catalytic reduction of oxygen by the heme proteins [43].

Fe_3O_4–CS–Hb/GCE also showed good catalytic activity toward hydrogen peroxide. When H_2O_2 was added to a pH 7.0 PBS, compared with the system without H_2O_2, the voltammograms of Fe_3O_4–CS–Hb/GCE showed a significant increase in the reduction peak at −0.41 V with the decreasement of the oxidation peak (Fig. 9). Moreover, the reduction peak increased gradually with the gradually addition of H_2O_2. The direct reduction of H_2O_2 at Fe_3O_4/GCE was hardly observed in the studied potential window (Fig. 9a), indicating the catalytic current resulted from the immobilized Hb. The mechanisms can be expressed as follows [44]:

$$Hb(Fe^{3+}) + H_2O_2 \rightarrow CompoundI(Fe^{4+}{=}O) + H_2O$$

$$CompoundI(Fe^{4+}{=}O) + e + H^+ \rightarrow CompoundII$$

$$CompoundII + e + H^+ \rightarrow Hb(Fe^{3+}) + H_2O$$

The current response was linear to the concentration of H_2O_2 in the range from 5 to 90 μmol L^{-1}. The regression equation is I (μA) = 1.59 + 0.026c (μmol L^{-1}) with a coefficient of 0.999. The sensitivity was 0.026 μA μM^{-1} and the detection limit was 5.0×10^{-7} mol L^{-1} based on S/N = 3, which was lower than that of 60 μM for a nickel oxide nanoparticles based H_2O_2 biosensor [12].

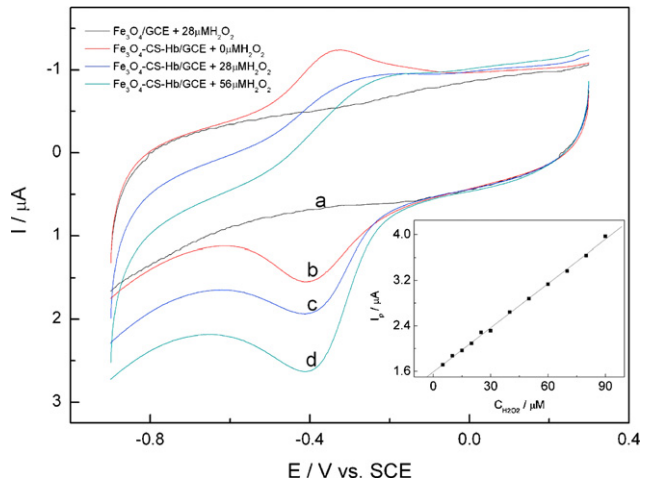

Fig. 9. Cyclic voltammograms of Fe_3O_4/GCE with 28 μM H_2O_2 (a), Fe_3O_4–CS–Hb/GCE without H_2O_2 (b) and with different H_2O_2 concentrations in 0.1 M pH 7.0 PBS at 200 mV s^{-1}: 28 μM (c) and 56 μM(d). Inset: Plot of catalytic peak current vs. the concentration of H_2O_2. Scan rate: 200 mV s^{-1}.

The electrocatalytic current (i_{cat}) linearly increased with increasing the concentration of H_2O_2 in the beginning and thereafter began to level off (Fig. 9 Inset), indicating that the relationship between i_{cat} and the concentration of H_2O_2 showed a Michaelis–Menten response. The apparent Michaelis–Menten constant (K_M^{app}), which can provide an indication of the enzyme–substrate kinetics, can be calculated according to Lineweaver–Burk equation [45]:

$$\frac{1}{I_{ss}} = \frac{1}{I_{max}} + \frac{K_M^{app}}{I_{max}C}$$

where I_{ss} is the steady-state current after the addition of substrate, C is the bulk concentration of substrate and I_{max} is the maximum current under saturated substrate solution. K_M^{app} can be obtained by the analysis of slope and intercept of the plot of the reciprocals of the steadystate current vs. H_2O_2 concentration. The Michaelis–Menten constant of the system (K_M^{app}) in this work can be calculated to be 38.1 μmol L^{-1} (calculated from the linear range in Fig. 9 Inset), implying that the Fe_3O_4–CS–Hb/GCE exhibited a higher affinity for hydrogen peroxide. As is well known the smaller K_M^{app} shows the higher catalytic ability. The value of K_M^{app} for Hb in this work was smaller than 1.4 mmol L^{-1}, the value obtained when Hb was adsorbed onto chitosan stabilized gold nanoparticles modified electrode [24], and also smaller than 83.3 μmol L^{-1} for a graphite electrode modified with a *N*,*N*-dimethylformamide film [46], which indicated that Hb entrapped in composite Fe_3O_4–CS–Hb film had good affinity to H_2O_2 and higher enzymatic activity toward H_2O_2 reduction.

3.7. *Stability and reproducibility of Fe_3O_4–CS–Hb/GCE*

We studied the storage stability of the sensor by storing it at 4 °C when not in use and measured intermittently. Eight days later the response of the composite electrode still retained its activity 92% of its initial value.

The reproducibility of the current response for the Fe_3O_4–CS–Hb/GCE was examined at a H_2O_2 concentration of 20 μM and the relative standard deviation was 2.5% for 10 independent determinations.

3.8. H_2O_2 determination in real sample

We investigated the concentration of H_2O_2 in eyedrops as real sample by means of the as-prepared H_2O_2 biosensor. The sample was diluted with pH 7.0 PBS to 30 μM. The concentration of H_2O_2 was calculated to be 29.86 μM by standard addition method. The recovery rate was calculated to be 99.5%. The result indicated that this method can be directly used to determine H_2O_2 in real samples. The phenomenon might be ascribed to the high selectivity of the biosensor.

4. Conclusions

Magnetic nanoparticles (Fe_3O_4) were successfully synthesized by a chemical coprecipitation method. It demonstrated that magnetic nanoparticles is an attractive material to immobilize Hb to achieve its direct electrochemistry on GCE. Redox peak currents increased linearly with the increase of scan rate, indicating a surface-controlled electrode process. The results indicated that Fe_3O_4–CS film was an attractive matrix to provide a favorable microenvironment for redox proteins and enzymes to undergo a facile electron transfer reaction and Hb entrapped in composite Fe_3O_4–CS–Hb film had good affinity to H_2O_2 and higher enzymatic activity toward H_2O_2 reduction. Thus it was expected to have widely potential applications in direct electrochemistry, biosensors and biocatalysis.

Acknowledgments

This work was supported by the National Natural Science Foundation of China (20775088) and the Foundation of State Key Laboratory of Environmental Chemistry and Ecotoxicology, Research Center for Eco-Environmental Sciences, Chinese Academy of Sciences (KF2008-06).

References

[1] J.F. Rusling, Acc. Chem. Res. 31 (1998) 363.
[2] F.A. Armstrong, G.S. Wilson, Electrochim. Acta 45 (2000) 2623.
[3] A. Heller, Acc. Chem. Res. 23 (1990) 128.
[4] S.F. Hou, K.S. Yang, H.Q. Fang, H.Y. Chen, Talanta 47 (1998) 561.
[5] L.N. Wu, M. McIntosh, X.J. Zhang, H.X. Ju, Talanta 74 (2007) 387.
[6] L.Z. Yang, H.Y. Liu, N.F. Hu, Electrochem. Commun. 9 (2007) 1057.
[7] D. Du, X. Huang, J. Cai, A.D. Zhang, J.W. Ding, S.Z. Chen, Anal. Bioanal. Chem. 387 (2007) 1059.
[8] J. Yang, N. Hu, Bioelectrochem. Bioenergy 48 (1999) 117.
[9] L. Shen, R. Huang, N.F. Hu, Talanta 56 (2002) 1131.
[10] H. Liu, N. Hu, Anal. Chim. Acta 481 (2003) 91.
[11] Y. Zhou, N. Hu, Y. Zeng, J.F. Rusling, Langmuir 18 (2002) 211.
[12] A. Salimi, E. Sharifi, A. Noorbakhsh, S. Soltanian, Electrochem. Commun. 8 (2006) 1499.
[13] G.L. Luque, M.C. Rodríguez, G.A. Rivas, Talanta 66 (2005) 467.
[14] Y.L. Liu, Y.H. Yang, H.F. Yang, Z.M. Liu, G.L. Shen, R.Q. Yu, J. Inorg. Biochem. 99 (2005) 2046.
[15] E. Topoglidis, C.J. Campbell, A.E.G. Cass, J.R. Durrani, Electroanalysis 18 (2006) 882.
[16] G. Zhao, J.J. Feng, J.J. Xu, H.Y. Chen, Electrochem. Commun. 7 (2005) 724.
[17] D.H. Chen, M.H. Liao, J. Mol, Catal. B Enzym. 16 (2002) 283.
[18] D. Cao, P. He, N. Hu, Analyst 128 (2003) 1268.
[19] P.A. Dresco, V.S. Zaitsev, R.J. Gambino, B. Chu, Langmuir 15 (1999) (1945).
[20] R.V. Mehta, R.V. Upadhyay, S.W. Charles, C.N. Ramchand, Biotechnol. Tech. 11 (1997) 493.
[21] M. Koneracka, P. Kopcansky, M. Antalik, M. Timko, C.N. Ramchand, D. Lobo, R.V. Mehta, R.V. Upadhyay, J. Magn. Magn. Mater. 201 (1999) 427.
[22] J. Dobson, FEBS Lett. 496 (2001) 1.
[23] P.P. Schultheiss-Grassi, R. Wessiken, J. Dobson, Biochim. Biophys. Acta 1426 (1999) 212.
[24] J.J. Feng, G. Zhao, J.J. Xu, H.Y. Chen, Anal. Biochem. 342 (2005) 280.
[25] E. Renbutsu, M. Hirose, Y. Omura, F. Nakatsubo, Y. Okamura, Y. Okamoto, H. Saimoto, Y. Shigemasa, S. Minami, Biomacromolecules 65 (2005) 2385.
[26] X.L. Luo, J.J. Xu, Y. Du, Anal. Biochem. 334 (2004) 284.
[27] Y. Zhou, H. Yang, H.Y. Chen, Talanta 76 (2008) 419.
[28] X.B. Lu, J.Q. Hu, X. Yao, Z.P. Wang, J.H. Li, Biomacromolecules 7 (2006) 975.
[29] H. Okuma, E. Watanabe, Biosens. Bioelectron. 17 (2002) 367.
[30] S.H. Baek, B. Kim, K.D. Suh, Colloids Surf. A: Physicochem. Eng. Aspects 316 (2008) 292.
[31] S. Ogawa, E.A. Decker, D.J. McClements, J. Agric. Food Chem. 52 (2004) 3595.
[32] G.D. Mendenhall, Y. Geng, J. Hwang, J. Colloid Interface Sci. 184 (1996) 519.
[33] J.J. Huang, Z.S. Xu, C.F. Yi, J. Hubei Univ. Nat. Sci. 291 (2007) 50.
[34] Z.H. Chi, S.A. Asher, Biochemistry 37 (1998) 2865.
[35] J.K. Kauppinen, D.J. Moffate, H.H. Mantsch, D.G. Lameron, Appl. Spectrosc. 35 (1981) 271.
[36] C.C. Silva, H.H.B. Rocha, F.N.A. Freire, M.R.P. Santos, K.D.A. Saboia, J.C. Goes, A.S.B. Sombra, Mater. Chem. Phys. 92 (2005) 260.
[37] E. Laviron, J. Electroanal. Chem. 101 (1979) 19.
[38] E. Laviron, J. Electroanal. Chem 100 (1979) 263.
[39] H.Y. Gu, A.M. Yu, H.Y. Chen, J. Electroanal. Chem. 516 (2001) 119.
[40] Y.D. Zhao, Y.H. Bi, W.D. Zhang, Q.M. Luo, Talanta 65 (2005) 489.
[41] A.M. Bond, Modern Polarographic Methods in Analytical Chemistry, Dekker, New York, 1980, p. 29.
[42] I. Yamazaki, T. Araiso, Y. Hayashi, H. Yamada, R. Makino, Adv. Biophys. 11 (1978) 249.
[43] C.P. Andrieux, C. Blocman, J.M. Fumas-Bouchiant, F.M. Halla, J.M. Saveant, J. Electroanal. Chem. 113 (1980) 19.
[44] H.Y. Xiao, H.X. Lu, H.Y. Chen, Anal. Biochem. 278 (2000) 22.
[45] J. Li, S.N. Tan, H. Ge, Anal. Chim. Acta 335 (1996) 137.
[46] Y.X. Xu, F. Wang, X.X. Chen, S.S. Hu, Talanta 70 (2006) 651.